Structural effects of hydrostatic pressure in orthorhombic $La_{2-x}Sr_xCuO_4$

H. Takahashi
Institute for Solid State Physics, University of Tokyo, 7-22-1 Roppongi, Tokyo 106, Japan

H. Shaked,* B. A. Hunter, P. G. Radaelli, R. L. Hitterman, D. G. Hinks, and J. D. Jorgensen
Materials Science Division, Argonne National Laboratory, Argonne, Illinois 60439
(Received 22 February 1994)

We have investigated the effect of hydrostatic pressure on the structure of orthorhombic $La_{2-x}Sr_xCuO_4$ between 1 atm and 0.6 GPa, using neutron powder diffraction. Increasing pressure causes the tilt angle of CuO_6 octahedra to decrease, leading to a transition to tetragonal symmetry. There is a strong compressibility anisotropy for the orthorhombic structure. Order parameters for the transition versus pressure are consistent with Landau theory for a second-order transition. It is shown that this transition can be universally scaled over (x,T,P) space in the context of Landau theory. We conclude that T_c varies inversely with the tilt angle and is maximum for the tetragonal structure, i.e., for flat and square CuO_2 planes, for this compound.

I. INTRODUCTION

The compound $La_{2-x}Sr_xCuO_4$ offers one of the best opportunities for investigating the relationship between crystal structure and superconductivity. As a function of increasing strontium content, there is a transition from orthorhombic to tetragonal symmetry. Within the orthorhombic phase, the tilt angle of CuO_6 octahedra depends on strontium content, varying smoothly to zero at the structural transition. The application of pressure also alters the tilt angle and produces the same structural transition at constant Sr content. Here we report the structural changes in orthorhombic $La_{2-x}Sr_xCuO_4$ produced by the application of hydrostatic pressure. When combined with other work, these results allow clear conclusions to be drawn about the effects of varying the tilt angle and the transformation to tetragonal symmetry on superconductivity in this compound.

For $La_{2-x}Sr_xCuO_4$, bulk superconductivity is observed in the composition range $0.07 \le x \le 0.24$. At low temperature (10–70 K) and ambient pressure, $La_{2-x}Sr_xCuO_4$ has an orthorhombic structure with space group *Bmab*[1,2] throughout most of this composition range ($x \le 0.21$). For $x \ge 0.21$, $La_{2-x}Sr_xCuO_4$ has a tetragonal structure with space group $F4/mmm$.[1,3] The orthorhombic-to-tetragonal (OT) transition line[4–6] is shown in Fig. 1. Superconductivity is observed in orthorhombic and tetragonal samples. However, the superconducting critical temperature T_C decreases rapidly as a function of x in the $0.21 < x < 0.24$ composition range, and other superconducting properties, like the Meissner fraction, can be depressed as well. Therefore, it has been important to investigate whether superconductivity in the tetragonal phase is an intrinsic phenomenon or results from the presence of structural or compositional inhomogeneities. Based on the observation of an abrupt change in the Meissner signal at the OT transition, Takagi *et al.* concluded that the structural transition was responsible for the loss of superconductivity.[4] However, in a similar experiment, Kitazawa *et al.* and Nagano *et al.* did not see any discontinuity in the Meissner signal, and concluded that bulk superconductivity exists in both the orthorhombic and tetragonal phases.[8,9] In a recent study on powder samples,[6] we presented structural and magnetic data which support the conclusions of Kitazawa and coworkers.

Measurements of the structural and superconducting properties at high pressure provide a means for investigating the issue of superconductivity in the tetragonal phase. It is known[10–14] that pressure has a strong effect on the structural properties of this compound: For orthorhombic samples, the application of hydrostatic pressure reduces both the orthorhombic strain[13] and the intensity of the characteristic *Bmab* reflections,[12] and ultimately induces a structural transition to the tetragonal phase. For example, at 39 K, the OT transition shifts from $x = 0.206$ at ambient pressure to $x = 0.16$ at 1.5 GPa.[14] Pressure is not expected to strongly affect the

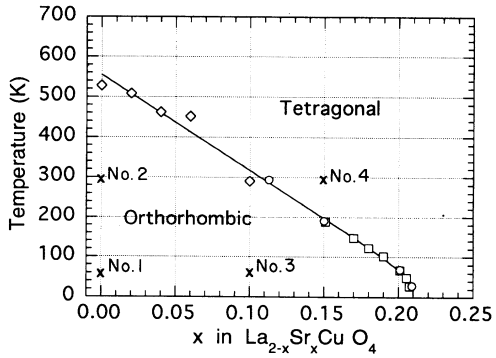

FIG. 1. The (x,T) plane in the phase diagram of $La_{2-x}Sr_xCuO_4$. The locations in this plane of the four experiments (see text) are indicated (× symbols). Measured points for the orthorhombic to tetragonal transition are shown as reported in Ref. 4 (○ symbols), Ref. 5 (◇ symbols), and Ref. 6 (□ symbols). The line is a best fit [Eq. (5)] to the reported points.

number of electronic carriers on the CuO_2 planes of this compound, which is thought to be proportional to the strontium concentration x, since $La_{2-x}Sr_xCuO_4$ does not have a "charge reservoir" layer that can exhibit a variable oxidation state as do the Cu-O chains in $YBa_2Cu_3O_{7-\delta}$. Therefore, a study of the structural and superconducting phase diagrams at various pressures should determine whether the change of crystal symmetry affects superconductivity. Recently, Yamada and Ido measured the T_C's of several $La_{2-x}Sr_xCuO_4$ samples ($0.15 \leq x \leq 0.22$) as a function of applied pressure ($0 \leq P \leq 2$ Gpa).[14] The OT phase transition temperature was also determined at each composition and pressure from the anomaly in the thermal expansion coefficient. Yamada and Ido established that T_C increases with pressure in the orthorhombic phase, reaching the maximum value at the OT phase transition. They found that in the tetragonal phase, T_C is essentially pressure independent. At 2 GPa, the shape of the T_C vs x curve is similar to that at ambient pressure: The maximum T_C is reached for $x \approx 0.15$ [raised from 38 K (ambient pressure) to 42 K (2 GPa)], and superconductivity disappears for $x > 0.24$. This study indicates that the proximity of the low-temperature OT transition line and the disappearance of superconductivity at ambient pressure is essentially accidental, and can be removed by the application of pressure. In addition, the steplike discontinuity in dT_C/dP (Ref. 14) at the OT transition (which is unique among high-T_C cuprates[15,16]) suggests that the increase in T_C with pressure in the orthorhombic phase may be related to a structural order parameter, which vanishes together with dT_C/dP at the transition, where the "optimal" superconducting structure is attained.

This observation suggests that the correlation between crystal structure and electronic structure and its possible influence on the superconducting properties should be investigated. Using band-structure calculations, Norman *et al.* have recently shown[17] that small structural distortions of the type associated with tilts of the CuO_6 octahedra in the orthorhombic structure do tend to lower the electronic density of states, but by only a small amount unless the tilt angle becomes large. They suggest, however, that such small changes may be sufficient to explain the observed pressure dependence of T_C. Clearly, detailed measurements of the structural parameters as a function of pressure are needed for a more quantitative analysis of the problem.

In this paper, we present structural refinements using neutron powder diffraction data for three measurements on orthorhombic samples [La_2CuO_4 at 60 K (experiment 1) and 295 K (experiment 2) and $La_{1.9}Sr_{0.1}CuO_4$ at 60 K (experiment 3), shown as points 1, 2, and 3 in Fig. 1] as a function of applied hydrostatic pressure ($0 \leq P < 0.6$ GPa). The structural parameters are compared with those obtained for a tetgragonal sample [$La_{1.85}Sr_{0.15}CuO_4$ at 295 K (experiment 4), point 4 in Fig. 1] reported previously.[7] From the structural measurements, the variation of order parameters associated with the OT transition are calculated and compared with Landau theory. The pressure-induced OT transition appears to be a well-behaved second-order transition. Thus, these results confirm that the tetragonal structure, where the CuO_6 octahedral tilt angle has been reduced to zero, displays the highest T_C for the $La_{2-x}Sr_xCuO_4$ system.

II. EXPERIMENT

$La_{2-x}Sr_xCuO_4$ ($x = 0.00$, 0.10) powder samples were synthesized as described previously.[6] After synthesis, the $x = 0.10$ sample was annealed at 700 °C in flowing oxygen, followed by slow cooling to room temperature. The $x = 0.00$ sample was annealed at 700 °C in flowing nitrogen, and then rapidly quenched to room temperature. These annealing conditions produce samples with oxygen contents close to 4.00.

Time-of-flight neutron powder-diffraction data were collected on the special environment powder diffractometer (SEPD) (Ref. 18) at Argonne's intense pulsed neutron source (IPNS). The SEPD was equipped with a helium pressure cell[19] mounted on a 12-W closed-cycle refrigerator (Displex). This apparatus allows the temperature of the sample to be controlled between 60 K and room temperature with an accuracy of ±0.1 K. The pressure cell design allows data collection between 0 and 0.6 GPa at a fixed scattering angle of $2\theta = \pm 90°$ with no Bragg scattering from the cell. It also offers the advantage of perfectly hydrostatic conditions, precise pressure measurements, and the ability to change pressure and temperature without having to move the sample. A detailed description of the experimental apparatus has been given elsewhere.[19]

Three separate experiments, 1, 2, and 3, with $x = 0.00$ at 60 K, $x = 0.00$ at 295 K, and $x = 0.10$ at 60 K were performed (Fig. 1). The conditions $x = 0.00$ at 295 K and $x = 0.10$ at 60 K result in nominally equal orthorhombic strains at zero pressure (~1%) but for a nonsuperconducting composition in the former case and superconducting composition in the latter. For each experiment, data were collected for approximately 4 h per pressure, at seven different pressures from 1 atm to 0.6 GPa. The data were analyzed using the Rietveld technique, using the IPNS time-of-flight Rietveld code.[20] Refinements were carried out using the nonstandard *Bmab* space group (isomorphous to the standard *Cmca*, No. 64),[1,2] and included 304 Bragg reflections over a d-spacing range of $0.7 \leq d \leq 3.6$ Å. Scattering amplitudes used[21] were (in units of 10^{-12} cm) 0827, 0.702, 0.7718, and 0.5805 for La, Sr, Cu, and O, respectively. The refined parameters included the lattice constants, all variable atom positions, isotropic thermal parameters for all atoms, and three peak width parameters. The refined structural parameters for the three experiments are listed in Tables I, II, and III. A portion of the Rietveld profile for the $La_{1.9}Sr_{0.1}CuO_4$ sample at 60 K (experiment 3) at 0.6 GPa is shown in Fig. 2.

III. RESULTS AND DISCUSSION

The relative changes of the lattice parameters a, b, and c and of the cell volume V as a function of pressure for the three measurements on orthorhombic samples and for the previously studied tetragonal sample[7] are shown in Fig. 3. The average compressibilities and compressibility

TABLE I. Structural parameters for experiment 1 (La_2CuO_4 at 60 K). Rietveld refinements were done in the orthorhombic space-group *Bmab* (No. 64) (Ref. 1). Atom positions are La/Sr at $8f(0,y,z)$, Cu at $4a(0,0,0)$,O(1) at $8e(\frac{1}{4},\frac{1}{4},z)$, and O(2) at $8f(0,y,z)$. Numbers in parentheses represent standard deviations of the last significant digit. The weighted profile (wp) and the expected (exp) agreement factors (Ref. 20) are given (in %) in the last two lines.

P (GPa)		0.000	0.100	0.201	0.303	0.408	0.508	0.603
a(Å)		5.3352(1)	5.3341(1)	5.331(1)	5.3321(1)	5.3308(1)	5.3299(1)	5.3290(1)
b(Å)		5.4160(1)	5.4137(1)	5.4113(1)	5.4092(1)	5.4070(1)	5.4049(1)	5.4026(1)
c(Å)		13.1058(1)	13.1040(2)	13.1019(2)	13.0997(2)	13.0975(3)	13.0951(2)	13.0932(2)
V(Å^3)		378.693(8)	378.403(9)	378.115(8)	377.827(9)	377.515(8)	377.234(9)	376.960(9)
La	y	0.0084(3)	0.0080(3)	0.0070(3)	0.0088(3)	0.0092(3)	0.0094(3)	0.0091(3)
	z	0.3616(1)	0.3618(1)	0.3619(1)	0.3619(1)	0.3620(1)	0.3621(1)	0.3618(1)
	B (Å^2)	0.00(2)	0.09(3)	0.03(2)	0.00(3)	0.03(3)	−0.08(3)	0.04(3)
Cu	B (Å^2)	0.04(2)	0.19(3)	0.18(3)	0.07(3)	0.17(3)	0.11(3)	0.12(3)
O(1)	z	0.0089(2)	0.0083(2)	0.0085(2)	0.0082(2)	0.0084(2)	0.0086(2)	0.0087(2)
	B (Å^2)	0.18(3)	0.28(4)	0.21(3)	0.28(4)	0.25(4)	0.23(4)	0.34(4)
O(2)	y	−0.0403(3)	−0.0402(3)	−0.0398(3)	−0.0397(3)	−0.0393(3)	−0.0388(3)	−0.0375(3)
	z	0.1834(1)	0.1834(1)	0.1834(1)	0.1832(1)	0.1832(1)	0.1827(1)	0.1831(1)
	B (Å^2)	0.35(2)	0.35(3)	0.33(3)	0.36(3)	0.35(3)	0.36(3)	0.44(3)
R_{wp} (%)		7.32	6.49	6.30	6.55	6.41	6.45	6.60
R_{exp} (%)		5.33	5.03	4.84	4.81	4.75	4.65	4.73

anisotropies for all samples are given in Table IV. The three measurements in the orthorhombic phase yield similar compressibilities. The a-axis compressibilities, κ_a, are comparable for the orthorhombic and tetragonal structures, while the b-axis compressibility, κ_b, is a factor of ~2 larger for the orthorhombic structures, resulting in a decrease of the orthorhombic strain with pressure [Fig. 4(a)]. As a consequence, there is a large in-plane compressibility anisotropy (κ_b/κ_a) for the three orthorhombic structures (2.07, 1.96, 2.35) (Table IV), [while in-plane compressibility is isotropic (by symmetry) in the tetragonal phase]. It is interesting that the c-axis compressibilities adjust in such a way that the volume compressibilities are the same in the orthorhombic and tetragonal phases [Table IV, Fig. 3(c)]. The orthorhombic strain and the square of the tilt angle decrease linearly

TABLE II. Structural parameters for experiment 2 (La_2CuO_4 at 295 K). Rietveld refinements were done in the orthorhombic space-group *Bmab* (No. 64) (Ref. 1). Atom positions are La/Sr at $8f(0,y,z)$, Cu at $4a(0,0,0)$,$O(1)$ at $8e(\frac{1}{4},\frac{1}{4},z)$, and O(2) at $8f(0,y,z)$. Numbers in parentheses represent standard deviations of the last significant digit. The weighted profile (wp) and the expected (exp) agreement factors (Ref. 20) are given (in %) in the last two lines.

P (GPa)		0.000	0.102	0.200	0.303	0.408	0.508	0.612
a (Å)		5.3560(1)	5.3546(1)	5.3532(1)	5.3522(1)	5.3511(1)	5.3500(1)	5.3488(1)
b (Å)		5.4044(1)	5.4018(1)	5.3997(1)	5.3975(1)	5.3950(1)	5.3925(1)	5.3905(1)
c (Å)		13.1491(2)	13.1463(2)	13.1438(2)	13.1414(2)	13.1387(2)	13.1366(2)	13.1344(2)
V (Å^3)		380.615(8)	380.248(9)	379.932(9)	379.631(9)	379.304(9)	378.987(9)	378.701(9)
La	y	0.0073(3)	0.0071(3)	0.0063(3)	0.0065(3)	0.0073(3)	0.0065(3)	0.0058(3)
	z	0.3614(1)	0.3614(1)	0.3614(1)	0.3615(1)	0.3614(1)	0.3615(1)	0.361\6(1)
	B (Å^2)	0.26(2)	0.29(3)	0.26(2)	0.24(3)	0.26(3)	0.32(3)	0.29(3)
Cu	B (Å^2)	0.29(3)	0.31(3)	0.31(3)	0.29(3)	0.30(3)	0.35(3)	0.29(3)
O(1)	z	0.0078(2)	0.0078(2)	0.0077(2)	0.0075(2)	0.0076(2)	0.0077(2)	0.0073(2)
	B (Å^2)	0.55(3)	0.52(4)	0.52(4)	0.56(4)	0.56(4)	0.62(4)	0.58(4)
O(2)	y	−0.0341(3)	−0.0339(3)	−0.0337(3)	−0.0337(3)	−0.0334(3)	−0.0323(3)	−0.0323(3)
	z	0.1834(1)	0.1836(1)	0.1835(1)	0.1833(1)	0.1832(1)	0.1835(1)	0.1831(1)
	B (Å^2)	0.96(3)	0.95(4)	0.95(4)	0.92(4)	0.91(4)	1.01(4)	0.94(4)
R_{wp} (%)		6.70	7.10	6.30	6.73	6.58	6.73	6.52
R_{exp} (%)		5.16	5.75	4.85	5.05	4.94	5.08	4.80

TABLE III. Structural parameters for experiment 3 ($La_{1.9}Sr_{0.1}CuO_4$ at 60 K). Rietveld refinements were done in the orthorhombic space-group *Bmab* (No. 64) (Ref. 1). Atom positions are La/Sr at $8f(0,y,z)$, Cu at $4a(0,0,0)$, O(1) at $8e(\frac{1}{4},\frac{1}{4},z)$, and O(2) at $8f(0,y,z)$. Numbers in parentheses represent standard deviations of the last significant digit. The weighted profile (wp) and the expected (exp) agreement factors (Ref. 20) are given (in %) in the last two lines.

P (GPa)		0.000	0.100	0.200	0.301	0.409	0.510	0.605
a (Å)		5.3260(1)	5.3249(1)	5.3239(1)	5.3229(1)	5.3219(1)	5.3212(1)	5.3203(1)
b (Å)		5.3713(1)	5.3691(1)	5.3668(1)	5.3643(1)	5.3621(1)	5.3599(1)	5.3579(1)
c (Å)		13.1641(2)	13.1614(2)	13.1593(2)	13.1569(2)	13.1548(1)	13.1524(2)	13.1503(2)
V (Å^3)		376.587(8)	376.288(8)	375.992(8)	375.676(8)	375.392(7)	375.117(6)	374.853(8)
La	y	0.0064(3)	0.0063(3)	0.0071(3)	0.0070(3)	0.0067(3)	0.0065(2)	0.0070(4)
	z	0.3613(1)	0.3614(1)	0.3612(1)	0.3613(1)	0.3613(1)	0.3621(1)	0.3615(1)
	B (Å^2)	0.08(2)	0.11(2)	0.05(2)	0.10(2)	0.15(2)	0.07(2)	0.04(2)
Cu	B (Å^2)	0.14(3)	0.13(3)	0.13(3)	0.13(3)	0.12(3)	0.10(3)	0.15(3)
O(1)	z	0.0068(2)	0.0066(2)	0.0065(2)	0.0067(2)	0.0060(1)	0.0062(1)	0.0062(2)
	B (Å^2)	0.28(3)	0.28(3)	0.28(3)	0.27(3)	0.25(2)	0.26(2)	0.25(3)
O(2)	y	−0.0308(3)	−0.0303(3)	−0.0290(4)	−0.0283(4)	−0.0286(3)	−0.0280(3)	−0.0267(4)
	z	0.1822(1)	0.1821(1)	0.1823(1)	0.1824(1)	0.1823(1)	0.1821(1)	0.1823(1)
	B (Å^2)	0.52(3)	0.52(3)	0.56(3)	0.54(3)	0.43(2)	0.47(2)	0.52(3)
R_{wp} (%)		7.06	6.57	6.43	6.56	5.30	4.55	6.38
R_{exp} (%)		5.34	4.30	4.92	4.81	3.77	2.75	4.59

with pressure (Fig. 4) as expected for a second-order phase transition.[22–25] The extrapolated pressure values at which the strain vanishes are 7.2 (2), 4.4 (2), 3.6 (1) for the three experiments. The corresponding points on the OT transition plane in the (x,P,T) space are (0, 7.2, 60), (0, 4.4, 295), and (0.1, 3.6, 60) in reasonable agreement with values extrapolated from published x-ray-diffraction results.[11–13]

Since the variation of T_C with pressure is markedly different for the orthorhombic and tetragonal phases[14] it is important to ask whether there are significant differences in the compressions of individual bonds or the pressure dependence of other features. For the two superconducting compositions (experiments 3 and 4, Table IV) the compression of the apical, Cu-O(2), bond is larger for the tetragonal phase (experiment 4), which clearly disagrees with early attempts[26,27] to correlate dT_C/dP with compression of this bond. The compression of the inplane, Cu-O(1), bond (Table IV) is significantly larger for the orthorhombic phase. Thus, our data are qualitatively consistent with the compression of this bond being related to dT_C/dP. However, it is difficult to explain how dT_C/dP decreases to zero (the data[14] shows $0<dT_C/dP<0.1$ K/GPa) upon transforming to the tetragonal phase, since the Cu-O(1) bond compression decreases by only about 30%. The only structural feature that correlates fully with the behavior of T_C versus pressure is the tilt angle, which decreases with increasing pressure in the orthorhombic phase, and is (by symmetry) zero in the tetragonal phase.

The decrease of the tilt angle with increasing pressure is counter intuitive. If the CuO_6 octahedra were rigid, one might expect that compression would be accommodated by coordinated tilting of the octahedra around their shared corners, but just the opposite occurs. Clearly, a full understanding of the unusual compression mechanism in orthorhombic $La_{2-x}Sr_xCuO_4$ would require expressing the total energy as a function of cell volume in terms of individual atom positions. However, it is possible to understand the behavior in simple physical terms by considering the response of the CuO_2 and La_2O_2 layers to pressure.

Structural transitions are a common feature of the lay-

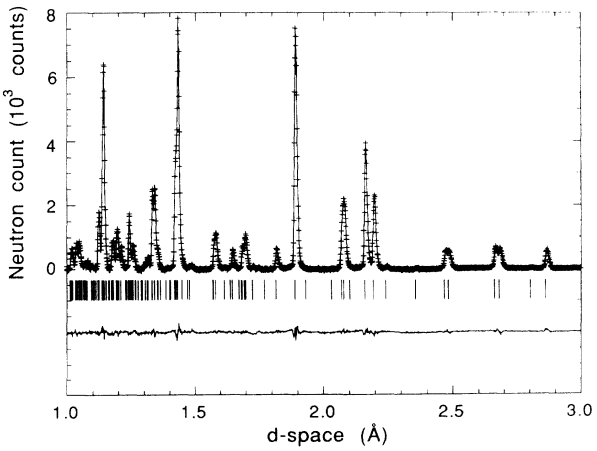

FIG. 2. Portion of the Rietveld refinement profile for the $La_{1.9}Sr_{0.1}CuO_4$ sample at 60 K (experiment 3) and 0.6 GPa. The plus symbols (+) are the raw time-of-flight neutron powder-diffraction data (collected for 3 h). The solid line is the calculated profile. The tick marks below the profile show the calculated positions of the allowed Bragg reflections. The background was fit as a part of the refinement, but has been subtracted prior to plotting. A difference curve (observed minus calculated) is plotted at the bottom.

ered copper oxide superconductors resulting from the mismatch between the CuO_2 layers and separating regions in the structure. In $La_{2-x}Sr_xCuO_4$, if the Cu-O(1) bond becomes too long in the tetragonal structure, the resulting mismatch between the CuO_2 layers and the La_2O_2 layers leads to a phase transition to orthorhombic symmetry (see Fig. 5). Thus, reduction of heavily-doped $La_{2-x}Sr_xCuO_4$ (by removing Sr) will lengthen the Cu-O(1) bond eventually leading to a lattice mismatch that is relieved by the transition to orthorhombic symmetry. The orthorhombic structure can accommodate a longer Cu-O(1) bond because of the additional degrees of freedom provided by the tilt and scissor distortion (the distortion of the equatorial plane of the octahedra which is a perfect square in the tetragonal phase and becomes rectangular in the orthorhombic phase). As a result, it is observed that the change in Cu-O(1) bond length on oxidation is considerably larger in the orthorhombic structure (−0.11 Å/Sr atom) than in the tetragonal structure (−0.02 Å/Sr atom).[6] Comparison of the compressibilities of the Cu-O(1) bonds in the orthorhombic and tetragonal phases (Table IV and Fig. 6) shows that Cu-O(1) bond compression is larger in the orthorhombic phase. Thus, the application of pressure is, in some sense, equivalent to adding Sr to the lattice. Both cause a reduction of the Cu-O(1) bond length with a resultant decrease of the tilt angle eventually leading to the tetragonal structure. Notice (Table IV) that $\kappa_a < \kappa_{\text{Cu-O(1)}} < \kappa_b$, whereas, $\kappa_c < \kappa_{\text{Cu-O(2)}}$ [i.e., the Cu-O(2) bond length is softer than the lattice constant c].

It is also instructive to view the compression behavior in terms of the response of the La_2O_2 layers. In the orthorhombic structure, the mismatch between the CuO_2 and La_2O_2 layers is accommodated by displacing the atoms in the La_2O_2 plane [La and O(2)] to produce long and short La-O(2) bonds along the b axis (see Fig. 5). The long La-O(2) bonds essentially result from the existence of "extra space" in the La_2O_2 layer. In the orthorhombic structure, compression is enhanced along the b axis because reduction of the b-axis lattice parameter simply results in a reduction of this "extra space;" i.e., along the b axis the unusually long La-O(2) bond does not resist compression to the same degree as do the La-O(2) bonds along the a axis. This concept is illustrated in Fig. 7,

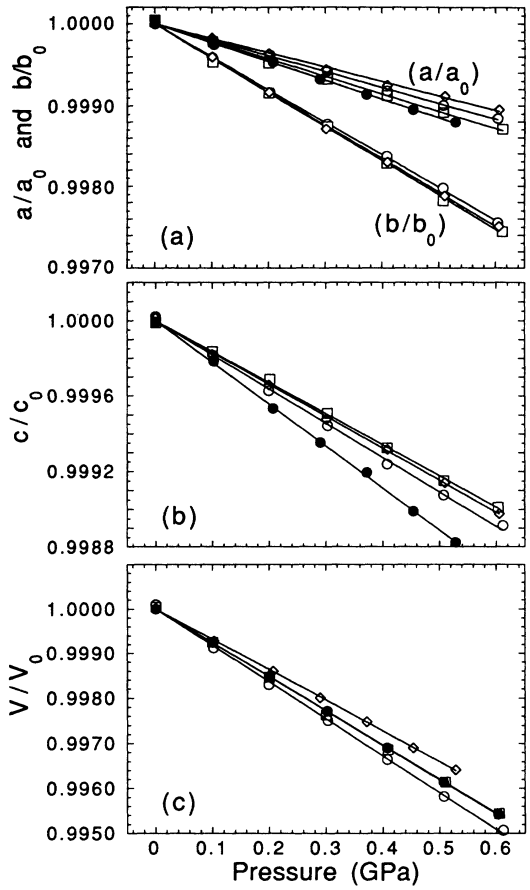

FIG. 3. The pressure dependence of the lattice parameters (a) and (b) and unit cell volume (c), normalized to their zero-pressure values. The different symbols represent different experiments as follows: (○) La_2CuO_4 at 60 K (experiment 1), (□) La_2CuO_4 at 295 K (experiment 2), (◇) $La_{1.9}Sr_{0.1}CuO_4$ at 60 K (experiment 3), (●) $La_{1.85}Sr_{0.15}CuO_4$ at 295 K (experiment 4, Ref. 7). Error bars are smaller than the symbols.

where the observed variation of La-O(2) bond distances with pressure is shown. With increasing pressure, the long La-O(2) bond decreases smoothly until it reaches a nominal value corresponding to the tetragonal phase [or corresponding to the La-O(2) bonds along the a axis in the orthorhombic phase]. At the same time, the short

TABLE IV. Linear compressibilities, compressibility anisotropies, volume compressibilities, bulk moduli, and compressibilities of the Cu-O(1) bonds. Numbers in parentheses represent standard deviations of the last significant digit.

	La_2CuO_4 at 60 K	La_2CuO_4 at 295 K	$La_{1.9}Sr_{0.1}CuO_4$ at 60 K	$La_{1.85}Sr_{0.15}Cu_4$ at 295 K
Experiment	1	2	3	4
κ_a (10^{-3} GPa^{-1})	1.95 (3)	2.15 (6)	1.77 (4)	2.29 (4)
κ_b (10^{-3} GPa^{-1})	4.03 (4)	4.22 (5)	4.14 (4)	2.29 (4)
κ_c (10^{-3} GPa^{-1})	1.63 (3)	1.83 (4)	1.70 (2)	2.21 (4)
κ_a/κ_c	1.20 (3)	1.18 (4)	1.04 (3)	1.04 (3)
κ_b/κ_c	2.48 (5)	2.31 (6)	2.44 (4)	1.04 (3)
κ_b/κ_a	2.07 (1)	1.96 (2)	2.35 (1)	1
κ (10^{-3} GPa^{-1})	7.59 (1)	8.2 (1)	7.60 (9)	6.8 (3)
B (GPa)	131.7 (2)	122(2)	132(2)	147(7)
$\kappa_{\text{Cu-O(1)}}$(10^{-3} GPa^{-1})	3.0 (2)	3.4 (1)	3.3 (1)	2.29 (4)

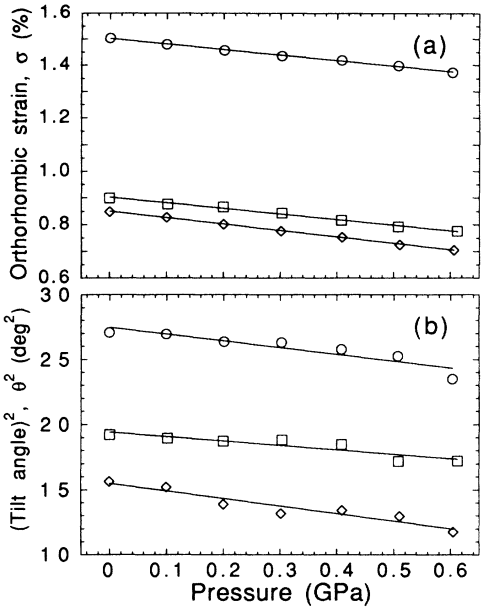

FIG. 4. The pressure dependence of the (a) orthorhombic strain, $\sigma=200\times(b-a)/(b+a)$, and (b) of the square of the CuO_6 octahedral tilt angle, θ^2, where $\theta=180\times y(O(2))\times b/[\pi\times z(O(2))\times c]$. The meaning of the symbols is the same as in Fig. 3. Error bars are nominally the size of the symbols.

La-O(2) bond along the b axis actually elongates with pressure (but at a smaller rate). Displacements of the O(1) atoms in the CuO_2 planes follow those of the O(2) atoms in such a way that the CuO_6 octahedra remain nearly rigid, leading to the concept of a tilt of the octahedra. The pressure-induced changes in the La_2O_2 plane described above result in a decrease of the tilt angle with increasing pressure (Fig. 4).

Although the foregoing discussion gives a simple physical picture of the response of the structure to hydrostatic pressure, it is not adequate for describing the details of

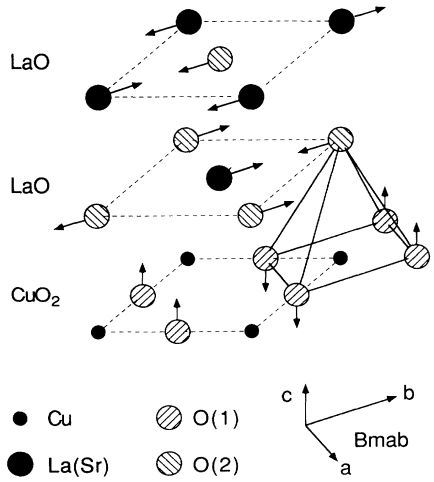

FIG. 5. Three atomic layers of the crystal structure of $La_{2-x}Sr_xCuO_4$. An idealized tetragonal structure, where the out of plane deviations are neglected, is shown. As the structure transforms from tetragonal ($F4/mmm$) to orthorhombic ($Bmab$), the atoms shift as shown.

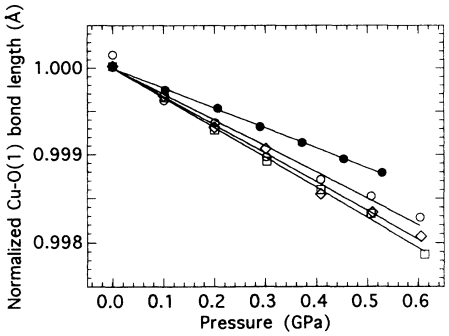

FIG. 6. The pressure dependence of the Cu-O(1) bond length for the four different experiments, normalized to their extrapolated zero-pressure value. The meaning of the symbols is the same as in Fig. 3.

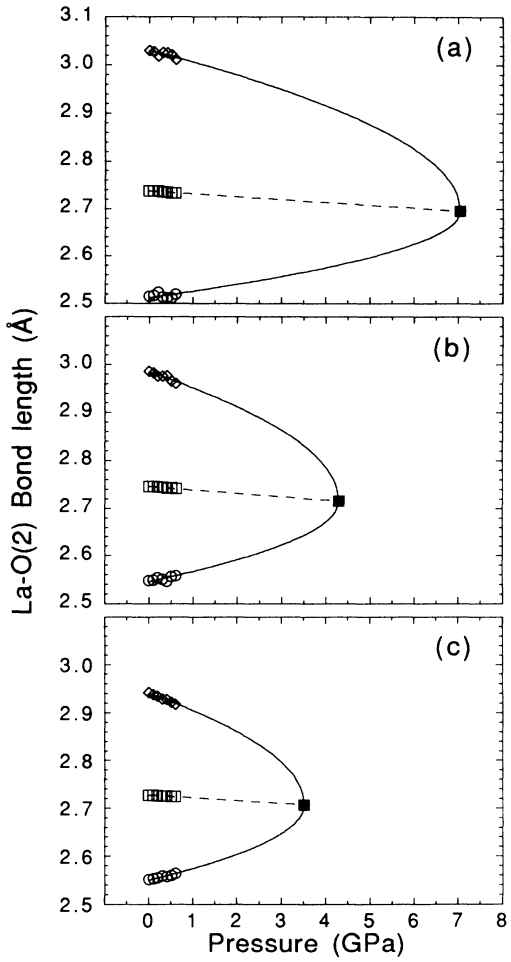

FIG. 7. The pressure dependence of the three intraplane La-O(2) bond lengths for (a) La_2CuO_4 at 60 K (experiment 1), (b) La_2CuO_4 at 295 K (experiment 2), and (c) $La_{1.9}Sr_{0.1}CuO_4$ at 60 K (experiment 3). Transition pressures, indicated by closed squares, as estimated by extrapolating the measured orthorhombic strain to zero (see text and Fig. 4). The La-O(2) bond length at this pressure is estimated by extrapolating the pressure dependence of the bonds nominally along the a axis (Fig. 5) that vary linearly with pressure. The solid lines represent parabolic fits passing through the zero-pressure and transition-pressure bond lengths. Error bars are smaller than the symbols.

the transition quantitatively. A more sophisticated description is provided by comparing the observed structural changes with Landau theory. The structural phase transitions in $La_{2-x}(Sr,Ba)_xCuO_4$ have been extensively analyzed in the framework of the Landau theory.[22-25] In particular, Ting, Fossheim, and Laegreid specifically discussed the dependence of the OT structural phase transition on pressure and composition.[24] They concluded that the effect of either pressure or composition can be phenomenologically ascribed to the coupling between the strain field created by applying pressure or changing the chemical composition and the structural order parameter. We have already shown in previous work[6] that the behavior of both the orthorhombic strain and the octahedral tilt angle as a function of composition is in agreement with the predictions of the Landau theory. Landau theory predicts a linear variation of the orthorhombic strain and a quadratic variation of the tilt angle[22-25] as a function of any external variable (composition, temperature, or pressure). The expected pressure dependence is seen in the present data (Fig. 4), although the pressure range is limited. This agreement suggests that it should be possible to compare data as a function of composition, temperature, or pressure as a function of an appropriate universal variable in the context of Landau theory.

The order parameter of the irreducible representation that describes the OT phase transition in $La_{2-x}(Sr,Ba)_xCuO_4$ is an axial vector. The direction of the order parameter coincides with the tilt axis, while its magnitude is proportional to the tilt angle.[6,22-25] If we consider solely the *Bmab-F4/mmm* phase transition (i.e., we ignore the possibility of other directions of the order parameter) the Landau excess free energy can be written to the fourth order as

$$\Delta F=-\tfrac{1}{2}c_1(T_S-T)\theta^2+c_2\theta^4+c_3\sigma\theta^2+\tfrac{1}{2}C_{66}\sigma^2 . \quad (1)$$

Here θ is the tilt angle, σ is the orthorhombic strain, C_{66} is the usual elastic constant, T_s is the phase transition temperature, and c_1, c_2, and c_3 are constants. This expression is expected to be valid at intermediate temperatures, and can be extended to low temperature by replacing T and T_s with an "effective" temperature:

$$T\rightarrow T^*=\Theta\coth\left[\frac{\Theta}{T}\right] , \quad (2)$$

where Θ has the dimension of a temperature and is related to the zero-point quantum fluctuations of the order parameter.[28] With the substitution in Eq. (2) we can model the low-temperature saturation of the quantities related to the order parameter (orthorhombic strain, tilt angles, etc.) and (as we shall see) the low-temperature behavior of the phase lines. Following the treatment of Ting and coworkers,[24] we can expand the effective critical temperature T_S^* to first order in pressure and composition:

$$T_S^*=T_0\left[1-\frac{P}{P_0}-\frac{x}{x_0}\right] , \quad (3)$$

where T_0, P_0, and x_0 are constants to be determined. Inserting Eqs. (2) and (3) into (1) we obtain

$$\Delta F=-\tfrac{1}{2}c_1T_0\left[1-\frac{T^*}{T_0}-\frac{P}{P_0}-\frac{x}{x_0}\right]\theta^2+c_2\theta^4 +c_3\sigma\theta^2+\tfrac{1}{2}C_{66}\sigma^2 . \quad (4)$$

Equation (4) shows that, once Θ, T_0, P_0, and x_0 are determined, the phase transition can be completely described in terms of the "universal" parameter $\xi=1-(T^*/T_0)-(P/P_0)-(x/x_0)$. In particular, the phase transition surface in the (x,P,T) space is defined by the equation

$$\xi=1-\frac{T^*}{T_0}-\frac{P}{P_0}-\frac{x}{x_0}=0 . \quad (5)$$

Therefore, Θ, T_0, P_0, and x_0 can be obtained by fitting experimentally determined OT phase transition lines. Using various literature data,[4-6] we have found a best fit to the OT phase transition line in the (x,T) plane at atmospheric pressure (Fig. 1). The refined values of the parameters varied in the fit are $\Theta=62(23)$ K, $T_0=557(9)$ K, and $x_0=0.236(7)$. From a similar fit of the phase transition line in the (x,P) plane at low temperature,[14] we have obtained $P_0=7.2(5)$ GPa. Equation (5) can be used to predict the position of the phase lines for other sections of the (x,P,T) space.

By minimizing the excess free energy in Eq. (4) as a function of θ and σ, we obtain

$$\theta^2\propto\sigma\propto\xi . \quad (6)$$

Therefore, plots of the orthorhombic strain and of the square of the tilt angle versus the universal parameter ξ should be straight lines. In Fig. 8, the orthorhombic strain is plotted versus ξ for a variety of measurements, including, composition-dependent data,[6] temperature-dependent data,[29] and pressure-dependent data (present work). The plot well approximates a straight line, with only a small deviation from linearity at high values of ξ.

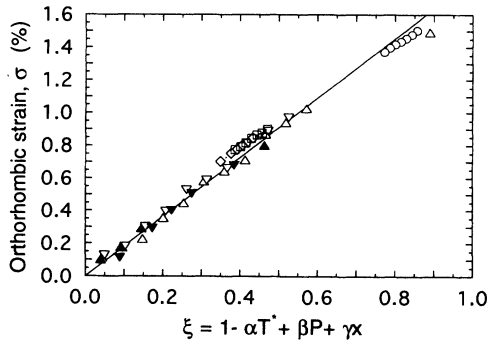

FIG. 8. The orthorhombic strain versus the "universal" parameter, ξ (see text). The results of the present work are represented by open circles, squares, and diamonds (meaning as in Fig. 3). Results from the literature which were obtained at ambient pressure are designated as follows: with $La_{2-x}Sr_xCuO_4(0\le x\le 0.3)$ samples, (Δ)—10 K (Ref. 6), (∇)—70 K (Ref. 6), (▲)—295 K (Ref. 6), and (▼)—a La_2CuO_4 sample with $334\le T\le 504$ K (Ref. 27). The solid line represents a linear fit to the data.

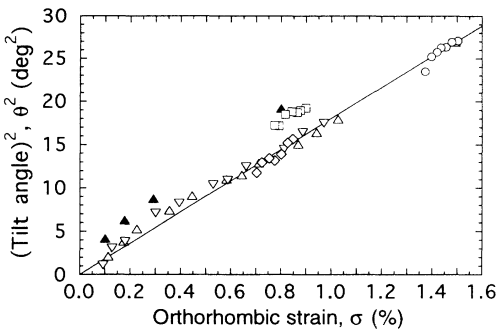

FIG. 9. Tilt angle squared, θ^2, vs orthorhombic strain, σ. The symbols have the same meaning as in Fig. 8. The high temperature data (▼) of Ref. 27, is omitted (see text). The solid line is a guide to the eye.

The data obtained in the pressure cell seem to display a small systematic upward shift, even at zero pressure. This small difference is likely due to the lower resolution of these data (from the 90° detector bank) with respect to all other data (from the backscattering 145° detector bank). In Fig. 9, the square of the tilt angle [as calculated from the apical oxygen O(2) displacement (Fig. 5)] is plotted versus the orthorhombic strain for the same data sets. The expected linear behavior is well reproduced at low temperature, but the tilt angle is higher than expected at higher temperatures. The simplest interpretation of this effect is as follows: Tilt angles are determined by the Rietveld method using both high-symmetry Bragg peaks (i.e., peaks that are allowed in both *Bmab* and *F4/mmm* space groups) and low-symmetry peaks (typical of *Bmab*). Low-symmetry peaks are mostly sensitive to the *coherent* part of the displacements (which determines the mean-field order parameter), while high-symmetry peaks are equally sensitive to *coherent* and *incoherent* displacements. The incoherent displacements are expected to increase with increasing temperature, due to thermal fluctuations. In fact, the incoherent displacements could, in principle, be modeled using highly anharmonic temperature factors. Therefore, at high-temperature, full-profile Rietveld refinements should yield higher-than-expected values of the tilt angles.

IV. CONCLUSIONS

We see that the behavior of the order parameters in the (x,P,T) space, corresponds to a well-behaved second-order phase transition between the well-known orthorhombic and tetragonal phases. Hence, it is the tetragonal phase where T_C reaches its highest value. We therefore conclude that T_C increases while the octahedral tilt angle decreases in the orthorhombic phase, and reaches its maximum at the OT phase transition where the tilt angle goes to zero. In the tetragonal phase the tilt angle remains zero, and T_C remains constant. These conclusions suggest that perfectly flat and square CuO_2 planes are the optimum structure for superconductivity.

ACKNOWLEDGMENTS

This work was supported by the National Science Foundation Office of Science and Technology Centers under Grant No. DMR 91-20000 (HS, BAH, PGR), the U.S. Department of Energy, Basic Energy Sciences–Materials Sciences, under Contract No. W-31-109-ENG-38 (RLH,DGH, and JDJ), the Ministry of Education, Science and Culture of Japan (HT), the Nuclear Research Center–Negev and Ben Gurion University in the Negev (HS).

*Permanent address: Department of Physics, Nuclear Research Center–Negev, P.O.B. 9001, Beer Sheva, Israel 84190 and Department of Physics, Ben-Gurion University of the Negev, P.O.B. 653, Beer Sheva, Israel 84105.

[1] *International Tables for Crystallography, Volume A, Space-Group Symmetry,* edited by T. Hahn (Reidel, Dordrecht, 1987), pp. 492 and 468.

[2] We use nonstandard *Bmab* setting rather than the standard *Cmca* setting in order to confirm with the standard *I4/mmm* setting in the tetragonal phase. In this setting the long lattice translation is along the *c* axis, which is the fourfold axis in the tetragonal phase.

[3] The tetragonal space group *F4/mmm* is identical to *I4/mmm*. The *F*-centered tetragonal unit cell conforms with the *B*-centered unit cell of the orthorhombic phase (it is two times larger than the *I*-centered tetragonal unit cell).

[4] H. Takagi, R. J. Cava, M. Marezio, B. Battlog, J. J. Krajewski, and W. F. Peck, Jr., Phys. Rev. Lett. **68**, 3777 (1992).

[5] M. Kato, Y. Maeno, and T. Fujita, Physica C **152**, 116 (1988).

[6] P. G. Radaelli, D. G. Hinks, A. W. Mitchell, B. A. Hunter, J. L. Wagner, B. Dabrowski, K. G. Vandervoort, H. K. Viswanathan, and J. D. Jorgensen, Phys. Rev. B **49**, 4163 (1994).

[7] S. Pei, J. D. Jorgensen, D. G. Hinks, B. Dabrowski, P. Lightfoot, and D. R. Richards, Physica C **169**, 179 (1990).

[8] K. Kitazawa, T. Nagano, Y. Nakayama, Y. Tomioka, and K. Kishio, Appl. Supercond. **1**, 567 (1993).

[9] T. Nagano, Y. Tomioka, Y. Nakayama, K. Kishio, and K. Kitazawa, Phys. Rev. B **48**, 9689 (1993).

[10] R. Moret, J. P. Pouget, and G. Collins, Europhys. Lett. **4**, 365 (1987).

[11] R. Moret, J. P. Pouget, C. Noguera, and G. Collins, Physica C **153-155**, 968 (1988).

[12] H. J. Kim and R. Moret, Physica C **156**, 363 (1988).

[13] J. Shu, J. Akella, J. Z. Liu, H. K. Mao, and L. W. Finger, Physica C **176**, 503 (1991).

[14] N. Yamada and M. Ido, Physica C **203**, 240 (1992).

[15] J. Wijingaarder and R. Griessen, in *Studies of High Temperature Superconductors,* edited by A. V. Narlikar (Nova, Commack, 1989), Vol. 2, p. 29.

[16] J. S. Schilling and S. Koltz, in *Physical Properties of High-Temperature Superconductors* (World Scientific, Singapore, 1992), Vol. 3, p. 59.

[17] M. R. Norman, G. J. McMullan, D. L. Novikov, and A. J.

Freeman, Phys. Rev. B **48**, 9935 (1993).
[18]J. D. Jorgensen, J. Faber, Jr., J. M. Carpenter, R. K. Crawford, J. R. Haumann, R. L. Hitterman, R. Kleb, G. E. Ostrowski, F. J. Rotella, and T. G. Worlton, J. Appl. Cryst. **22**, 321 (1989).
[19]J. D. Jorgensen, S. Pei, P. Lightfoot, D. G. Hinks, B. W. Veal, B. Dabrowski, A. P. Paulikas, R. Kleb, and I. D. Brown, Physica C **171**, 93 (1990).
[20]R. B. von Dreele, J. D. Jorgensen, and C. J. Windsor, J. Appl. Crystallogr. **15**, 581 (1982).
[21]*International Tables for Crystallography, Volume C, Mathematical, Physical and Chemical Tables,* edited by A. J. C. Wilson (Reidel, Dordrecht, 1983), p. 384.
[22]J. D. Axe, A. H. Moudden, D. Hohlwein, D. E. Cox, K. M. Mohanty, A. R. Moodenbaugh, and Y. Xu, Phys. Rev. Lett. **62**, 2751 (1989).
[23]D. Sahu and T. F. George, Solid State Commun. **65**, 1371 (1988).
[24]W. Ting, K. Fossheim, and T. Laegreid, Solid State Commun. **80**, 47 (1991).
[25]J. D. Axe (unpublished).
[26]C. Murayama, N. Mori, S. Yomo, H. Takagi, S. Uchida, and Y. Tokura, Nature **339**, 293 (1989).
[27]E. Kaldis, P. Fischer, A. W. Hewat, E. A. Hewat, J. Karpinski, and S. Rusiecki, Physica C **159**, 668 (1989).
[28]E. K. H. Salje, in *Phase Transitions in Ferroelastic and Coelastic Crystals* (Cambridge University Press, Cambridge, UK, 1990), Vol. 1, p. Ai-Aiii.
[29]P. G. Radaelli, J. D. Jorgensen, R. Kleb, B. A. Hunter, F. C. Chou, and D. C. Johnston, Phys. Rev. B **49**, 6239 (1994).